Archives of Advances in Biosciences

Original Article:

Conjugation of a Podoplanin-specific Single-chain Fragment Variable (scFv) to Granzyme B for Designing a Potential Therapeutic Against Malignant Tumors: An In-silico Experiment

Seyed Mohamad Javad Mirarefin[1*]

1. Department of Immunology, Faculty of Medical Sciences, Tarbiat Modares University, Tehran, Iran.

Cite this article as: Mirarefin SMJ, Conjugation of a Podoplanin-specific Single-chain Fragment Variable (scFv) to Granzyme B for Designing a Potential Therapeutic Against Malignant Tumors: An In-silico Experiment. 2024; 15:E44359. https://doi.org/10.22037/aab.v15i. 44359

https://journals.sbmu.ac.ir/aab/article/view/44359

Article info:
Received: 27 Dec 2023
Accepted: 27 Feb 2024
Published: 01 Apr 2024

*** Corresponding author:**

Seyed Mohamad Javad Mirarefin, Ph.D

Address: Department of Immunology, Faculty of Medical Sciences, Tarbiat Modares University, Tehran, Iran.

E-mail:
smj.mirarefin1994@gmail.com

Abstract

Introduction: Monoclonal antibodies (mAbs) and antibody-drug conjugates (ADCs) have changed the face of cancer treatment methods drastically. Herein, I attempted to conjugate a podoplanin (PDPN)-single-chain fragment variable (scFv) to granzyme B (GrB) to design an antibody conjugate (named LpMab-2-(G_4S)3-GrB) using in-silico techniques.

Materials and Methods: The 3D models of the PDPN-specific scFv (LpMab-2), LpMab-2-(G_4S)3-GrB, and PDPN were predicted by GalaxyWEB, assessed through Ramachandran plot analysis, and refined by 3Drefine. The physicochemical properties, solubility value, and Tm of LpMab-2-(G_4S)3-GrB were estimated/predicted and compared with LpMab-2 and GrB. Finally, the binding capacity of LpMab-2-(G_4S)3-GrB to PDPN was compared with that of LpMab-2 through docking and affinity prediction alongside identifying the residues that participate in the binding through 2D interaction plots using the LigPlot+ software.

Results: The 3D models were predicted to be of high quality and refined successfully. The solubility and Tm of LpMab-2 were predicted to decrease and increase following its conjugation with GrB, respectively, whereas its estimated half-life was not affected. The docking results indicated that LpMab-2-(G_4S)3-GrB targets PDPN in the same orientation as that of LpMab-2 and with the exact same residues as indicated by their 2D plots. Moreover, the affinity of LpMab-2-(G_4S)3-GrB to PDPN was predicted to be similar to that of the single scFv.

Conclusion: The conjugation of LpMab-2 to GrB does not affect its binding capacity or characteristics in a major negative fashion. In-silico techniques could be utilized for antibody engineering, and future studies could focus on the assessment of LpMab-2-(G_4S)3-GrB *in vitro* and *in vivo*.

Keywords: Antibody-drug conjugate, Cancer immunotherapy, Granzyme B, Podoplanin, Single-chain fragment variable

1. Introduction

The advent of monoclonal antibodies (mAbs) has changed the landscape of cancer treatment. Since the approval of the first mAb by the United States Food and Drug Administration (FDA), mAbs have experienced an increase in development and application in clinics. The conjugation of mAbs for the development of antibody-drug conjugates (ADCs) has also been considered as another revolution in the fight against malignancies. This strategy combines the cytotoxic effect of the conjugated drug with the specificity of the selected mAb to minimize the off-tumor effects of the drug as a single regimen. So far, numerous ADCs have entered the clinics for the treatment of patients with solid tumors (e.g., ado-trastuzumab emtansine) or blood-based cancers (e.g., polatuzumab vedotin) [1, 2].

As a heavily O-glycosylated protein with an approximate weight of 40 kDa, podoplanin (PDPN) is mainly expressed by the lymphatic endothelium [3]. Recently, PDPN has received a great deal of attention due to its clinical significance in gliomas, malignant mesothelioma, and squamous cell carcinomas [3]. Numerous researchers have considered PDPN a target antigen for the development of various treatment modalities. To date, a large number of PDPN-specific mAbs (such as NZ-1) and scFvs (such as 237Ab and LpMab-2) as well as PDPN-redirected chimeric antigen receptor (CAR)-T cells have been developed and assessed *in vitro* and preclinical studies [3-5].

Cytotoxic T cells exert their cytotoxic effects against target cells following the establishment of immunological synapses with the peptide-bound major histocompatibility complexes (pMHC) presented on the surface of target cells. This occurrence results in the secretion of perforin and granzyme B (GrB) which consequently leads to the cytolysis of the targeted cell [6]. Following its entrance into the target cells, GrB mediates the cleavage and activation of caspases 8 and 10, and caspases 3 and 7 resulting in the death of the targeted cells through the apoptosis process [6]. Therefore, GrB could be leveraged for therapeutic purposes as a potent cytotoxic agent through its conjugation with other targeting moieties such as VHHs, scFv, and even full-length mAbs [6]. The current study focuses on the design and characterization of a PDPN-specific antibody conjugate composed of a PDPN-specific scFv conjugated to GrB through a flexible linker peptide using in-silico techniques.

2. Materials and Methods

Sequences and 3D structures

The sequence of the PDPN-specific scFv was obtained from its related US patent (publication number: US20160347834A1; referred to as LpMab-2) (Figure 1A). The protein data bank (PDB) of GrB was retrieved from RSCB Protein Data Bank; accession number: 1FQ3), and its related amino acid sequence was also aligned and confirmed with that of the UniProt server; accession number: P10144) (Figure 1B). The signal peptide of GrB was removed from its sequence before its conjugation with the PDPN-specific scFv. The conjugated therapeutic was composed of LpMab-2 linked to the N-terminus of GrB via a $(G_4S)3$ linker (hereafter referred to as LpMab-2-$(G_4S)3$-GrB). This linker was chosen owing to its high degree of flexibility. The amino sequence of PDPN was retrieved from the UniProt server (accession number: Q86YL7), and its extracellular domain was used for the rest of the experiments (Figure 1C).

3D structure prediction and quality assessments

For the 3D modeling of the LpMab-2, LpMab-2-$(G_4S)3$-GrB, and PDPN, the GalaxyWEB modeling server was utilized [7]. The 3D model of each protein was predicted based on homology modeling with templates sharing a high degree of similarity [7]. The most favorable predicted models were selected and their quality was assessed using SWISS-MODEL's QMEANDisCo [8]. Moreover, further quality assessments through Ramachandran plot analysis were carried out by utilizing the MolProbity server [9]. The Ramachandran plot provides information with regard to amino acid residues in the favored regions, allowed regions, and outlier regions of a given 3D protein structure.

3D structural refinement through energy minimization

For refining the 3D structure of the predicted models, the structural refinement server of 3Drefine was utilized [10]. This server helps resolve errors that have occurred in the process of structure prediction by the modeling server. The Root Mean Square Deviation (RMSD) of each 3D model before and after energy minimization was calculated using the PyMOL software (Schrödinger, Inc., United States). All structural visualizations were also carried out using PyMOL.

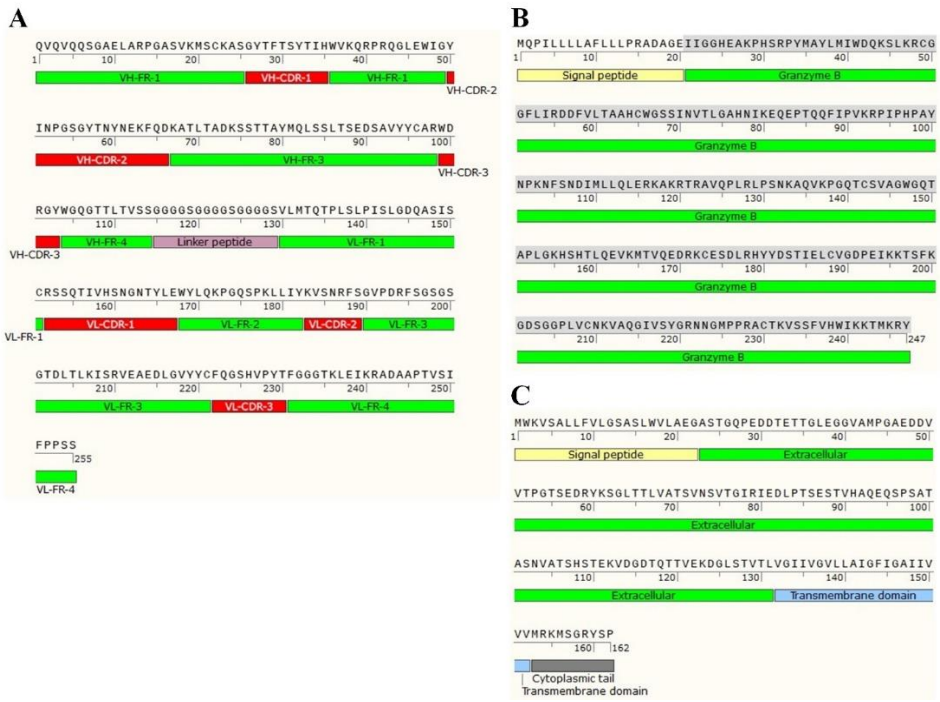

Figure 1. The amino acid sequences of LpMab-2 **(A)**, GrB **(B)**, and PDPN **(C)**.

Physicochemical properties

To ensure that LpMab-2-(G_4S)3-GrB has favorable physicochemical characteristics and that the conjugation of LpMab-2 to GrB has no negative impacts on such characteristics, the server of ProtParam was utilized. This server uses the amino acid sequence of any given protein as input to calculate various physicochemical properties such as molecular weight, half-life, and theoretical pI. Other important properties were also predicted which included solubility index and melting temperature using the Protein-Sol server and the Tm Predictor server, respectively [11].

Docking

Targeting and elimination of PDPN-positive tumor cells is achievable only if LpMab-2-(G_4S)3-GrB is still capable of recognizing and binding PDPN with a similar affinity to that of LpMab-2. To assess the binding capacity of LpMab-2 to PDPN and LpMab-2-(G_4S)3-GrB to PDPN, the docking server of ClusPro was taken into consideration [12, 13]. Moreover, the output of the docking step was further used in the prediction of the binding affinity of LpMab-2 to PDPN and LpMab-2-(G_4S)3-GrB to PDPN using the PRODIGY server (accessible at [14]. Furthermore, to identify the amino acid residues that participate in the binding of LpMab-2 to PDPN and LpMab-2-(G_4S)3-GrB to PDPN, 2D interaction plots of the docking complexes were illustrated using the LigPlot+ software.

3. Results

3D models of LpMab-2, LpMab-2-GSSSS3-GrB, and PDPN

The 3D models of LpMab-2, LpMab-2-(G_4S)3-GrB, and PDPN were predicted by the GalaxyWEB server successfully (Figure 2). For the modeling process of LpMaB-2, the server used 5I4F_A and 5VF2_A as templates whereas for the 3D structure prediction of LpMab-2-(G_4S)3-GrB, 1IAU_A, 5I4F_A, and 5VF2_A were used. It is noteworthy that 3REA_A was used as a template for the 3D modeling of PDPN. Next, the structural quality of these models was further analyzed (Table 1). According to the result of the QMEANDisCo server, the structural quality of LpMab-2 and LpMab-2-(G_4S)3-GrB was leaning toward favorable. However, the structural quality of PDPN showed a different pattern from the other two proteins (0.30 ± 0.08 for PDPN). The reason for this occurrence can be attributed to the lack of a crystallized structure of PDPN or the low similarity rate between PDPN and proteins whose 3D structures are known through different techniques.

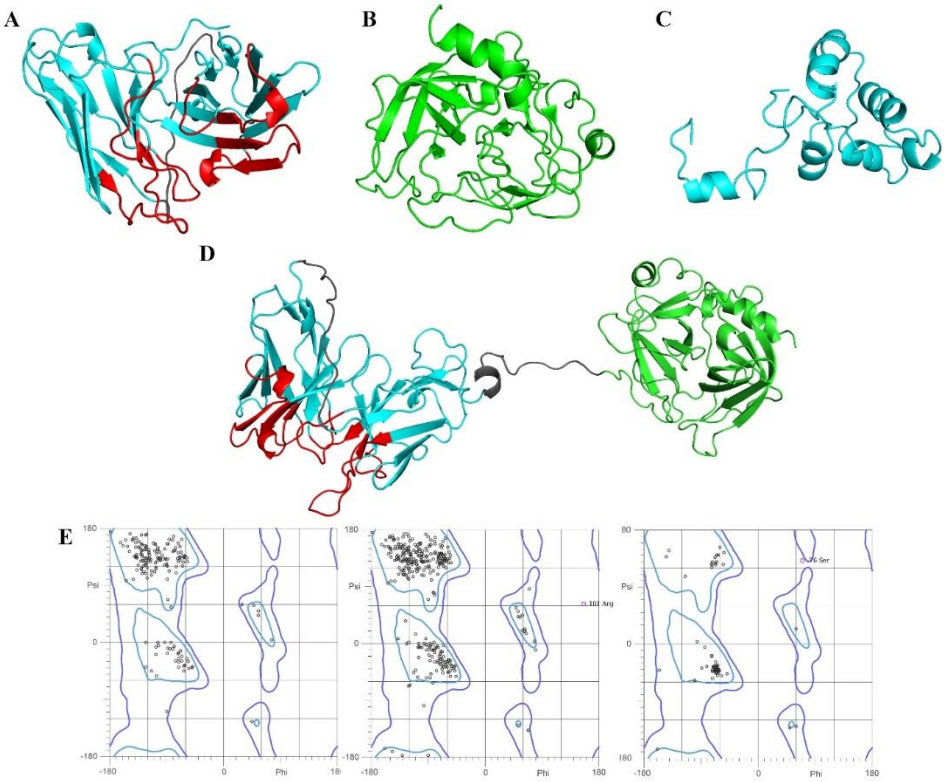

Figure 2. The 3D structures of LpMab-2, GrB, PDPN, and LpMab-2-(G4S)3-GrB, and the Ramachandran plots of the predicted 3D models. **A:** LpMab-2 in cartoon presentation. Frameworks are presented in cyan, CDRs in red, and the peptide linker in grey. **B:** GrB in cartoon presentation. **C:** PDPN in cartoon presentation. **D:** LpMab-2-(G4S)3-GrB in cartoon presentation. Frameworks are presented in cyan, CDRs in red, (G_4S)3 linkers in grey, and GrB in green. **E:** The Ramachandran plots of the predicted models of LpMab-2, LpMab-2-(G4S)3-GrB, and PDPN (left, middle, and right panel, respectively).

Table 1. Evaluation of the structural quality of the predicted 3D models of LpMab-2, LpMab-2-(G4S)3-GrB, and PDPN.

	LpMab-2	LpMab-2-GSSSS3-GrB	PDPN
QMEANDisco (0, bad; 1, good)	0.77 ± 0.05	0.77 ± 0.05	0.30 ± 0.08
Residues in favored regions (%)	96.4% (244/253)	96.0% (475/495)	94.4% (101/107)
Residues in allowed regions (%)	99.6% (252/253)	99.4% (492/495)	99.1% (106/107)
Residues in outlier regions (%)	0.40% (1/253)	0.61% (3/495)	0.93% (1/107)

With regard to the Ramachandran plot analysis (Table 1 and Figure 2E), the results indicated that the predicted 3D models of LpMab-2, LpMab-2-(G_4S)3-GrB, and PDPN are all of high quality, with more than 99% of the residues being in the allowed regions, and only 0.40, 0.61, and 0.93% of the residues of these models being in the outlier regions, respectively. Following energy minimization of LpMab-2 and LpMab-2-(G_4S)3-GrB, the RMSD of the aligned structure of LpMab-2 and GrB to LpMab-2-(G_4S)3-GrB was calculated to be 0.198 and 0.516 Ångström (Å), respectively (Figure 3A). These results demonstrated that the conjugation of LpMab-2 to GrB via the (G_4S)3 linker peptide does not negatively influence the structure, and consequently the function of LpMab-2 or GrB.

Characterization of LpMab-2-(G4S)3-GrB

The physicochemical characteristics of LpMab-2, GrB, and LpMab-2-(G_4S)3-GrB were determined as presented in Table 2. As expected, following the conjugation of LpMab-2 to GrB, the molecular weight of the scFv increased from ~ 27 to 53.7 kDa. Moreover, the theoretical pI of LpMab-2 increased from 8.94 to 9.44 following its conjugation with GrB. On the contrary, there was no difference between the estimated half-life of LpMab-2 in comparison with

Table 2. The physicochemical properties of LpMab-2, GrB, and LpMab-2-(G4S)3-GrB

		LpMab-2	GrB	LpMab-2-(G4S)3-GrB
Molecular weight		27247.31	25539.52	53714.67
Theoretical pI		8.94	9.69	9.44
Formula		$C_{1202}H_{1851}N_{329}O_{382}S_7$	$C_{1131}H_{1798}N_{330}O_{319}S_{13}$	$C_{2366}H_{3698}N_{674}O_{718}S_{20}$
Estimated half-life	In vitro	0.8 hours	20 hours	0.8 hours
	In yeast	10 min	30 min	10 min
	In *Escherichia coli*	10 hours	>10 hours	10 hours
Aliphatic index		64.24	71.72	65.71
Predicted Tm		55°C~65°C	higher than 65°C	higher than 65°C

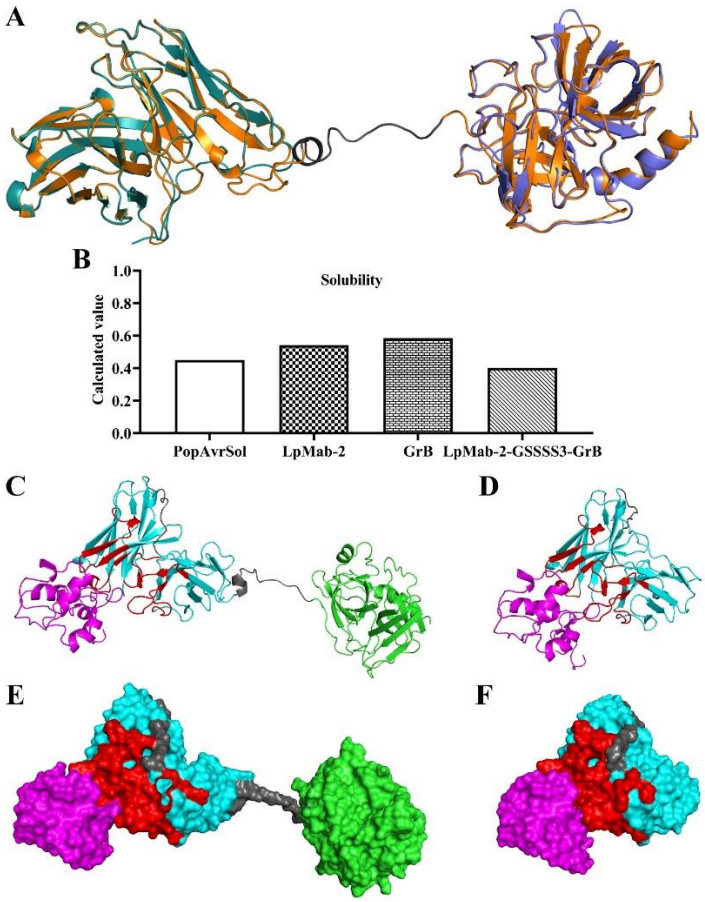

Figure 3. Structural alignment of LpMab-2 and GrB with LpMab-2-(G4S)3-GrB, the predicted solubility index, and the results of the ClusPro server for the docking of LpMab-2-(G4S)3-GrB and LpMab-2 to PDPN. **A:** The structural alignment of the 3D models of LpMab-2 (presented in deep teal) and GrB (presented in slate) with LpMab-2-(G4S)3-GrB (presented in orange) following the energy minimization of the predicted models. **B:** The predicted solubility of LpMab-2-(G4S)3-GrB in comparison with LpMab, GrB, and average soluble *E. coli* proteins (PopAvrSol). **C** and **D:** The docking complex of LpMab-2-(G4S)3-GrB to PDPN and LpMab-2 to PDPN in cartoon presentation, respectively. Framework regions are in cyan, linker peptides in grey, CDRs in red, and PDPN in magenta. **E** and **F:** The docking complex of LpMab-2-(G4S)3-GrB to PDPN and LpMab-2 to PDPN in surface model presentation, respectively. Framework regions are in cyan, linker peptides in grey, CDRs in red, and PDPN in magenta.

that of LpMab-2-(G_4S)3-GrB *in vitro*, in yeast, and in *Escherichia coli*. An increasing pattern was observed in the predicted Tm of LpMab-2 following its conjugation with GrB as its Tm increased from ~ 55-65 to > 65 °C. Additionally, the Protein-Sol server was also employed for the prediction of the scaled

solubility of LpMab-2, GrB, and LpMab-2-(G_4S)3-GrB. The server predicted the solubility index of LpMab-2, GrB, and LpMab-2-(G_4S)3-GrB as 0.542, 0.585, and 0.402, respectively (Figure 3B). According to the Protein-Sol server, the population for average *E. coli* proteins (PopAvrSol) is set as 0.45; therefore, any predicted solubility index more and less than 0.45 is predicted to be more and less soluble than average *E. coli* proteins, respectively. In this regard, conjugation of LpMab-2 to GrB is predicted to negatively impact the solubility of the conjugate to a less soluble state.

The binding of LpMab-2 and LpMab-2-(G4S)3-GrB to PDPN

According to the results obtained from the used docking server, it was predicted that both LpMab-2 and LpMab-2-(G_4S)3-GrB tend to target PDPN in a very similar orientation and at a similar epitope (Figure 3C, D, E, and F). More in-depth analysis indicated that the amino acids that participate in the binding of LpMab-2 to PDPN are the exact same residues that participate in the binding of LpMab-2-(G_4S)3-GrB to PDPN (Figure 4A and B), implying that conjugation of LpMab-2 to GrB does not affect its native binding site. Other results were consistent with these findings as the PRODIGY server predicted similar dissociation constants (K_d) for both LpMab-2-(G_4S)3-GrB docked to PDPN and LpMab-2 docked to PDPN from 25 to 37 ºC (Figure 4C). The predicted K_d decreased with an increase in temperature from 25 to 37 ºC which could be translated as a negligible affinity decline. Moreover, the PRODIGY server predicted the ΔG of LpMab-2-(G_4S)3-GrB docked to PDPN and LpMab-2 docked to PDPN as -9.7 (kcal mol^{-1}) which did not fluctuate with the increasing of temperature from 25 to 37 ºC.

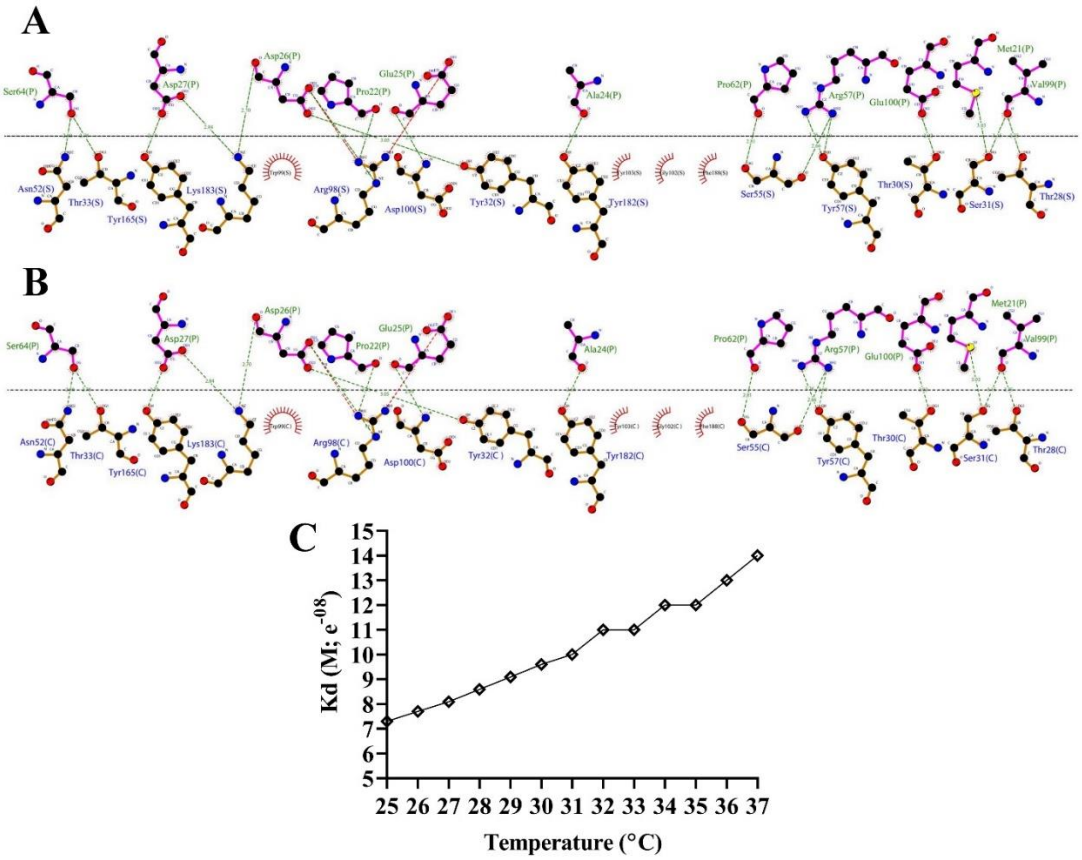

Figure 4. 2D plots of the amino acid residues of LpMab-2 and LpMab-2-(G4S)3-GrB that participate in their docking to PDPN, and the predicted K_d of LpMab-2 and LpMab-2-(G4S)3-GrB to PDPN. **A:** LpMab-2. The scFv is presented in the "S" chain (below the dashed line) whereas PDPN is presented in the "P" chain (above the dashed line). **B:** LpMab-2-(G4S)3-GrB. The conjugate is presented in the "C" chain (below the dashed line) whereas PDPN is presented in the "P" chain (above the dashed line). **C:** The predicted K_d of LpMab-2 and LpMab-2-(G4S)3-GrB to PDPN from 25 to 37 ºC. A similar pattern was observed for both LpMab-2 and LpMab-2-(G4S)3-GrB.

4. Discussion

mAbs and ADCs have given hope to patients with a broad range of malignancies, especially in solid tumors where adoptive cell therapy failed to deliver therapeutic benefits. In this regard, researchers should deeply focus on designing and developing novel antibody conjugates against suitable target antigens associated with malignancies. As a novel target antigen, PDPN has been known to have an elevated expression level in epithelial cells, T cells, and macrophages in inflammatory conditions (including psoriasis and rheumatoid arthritis) and oncological indications [3, 15]. In the tumor microenvironment (TME), an elevated expression level of PDPN has also been reported in the tumor stroma by various cellular elements such as cancer-associated fibroblasts [16]. This molecule has also been known to act as a co-inhibitory receptor on T lymphocytes which further accentuates its engagement in the invasion of malignant tumors [16]. All of the mentioned characteristics and roles of PDPN alongside its pronounced expression in numerous solid tumors (inclusive of glioblastoma, malignant mesothelioma, and angiosarcomas) render this molecule an interesting target antigen for the development of different treatment modalities. Herein, we employed precise in-silico techniques to design and develop an antibody conjugate composed of the PDPN-specific scFv LpMab-2 conjugated to GrB via a flexible GSSSS3 linker. The flexibility of this linker peptide allows the scFv to target its epitope on PDPN without being hampered by GrB. The PDPN-specific scFv LpMab-2 was chosen for this study owing to its capacity to bind with PDPN. In 2014, Kato and Kaneko developed LpMab-2 and reported that it was capable of reacting with PDPN-proficient cancer cells while being unreactive toward healthy cells [5]. Furthermore, these researchers suggested that LpMab-2 could be applied for the treatment of PDPN-proficient tumors [5]. Researchers have targeted PDPN-expressing tumors with other treatment modalities. Briefly, Shiina and fellow researchers developed PDPN-redirected CAR-T cells and demonstrated that these engineered cells were tumoricidal against PDPN-expressing tumor cells *in vitro* [17]. Moreover, it was reported that these CAR-T cells mediated tumor regression in xenograft mouse models of glioma following adoptive transfer [17]. According to another study, Abe and collaborators assessed the therapeutic effects of a PDPN-specific mAb, named NZ-12, in xenograft mouse models of malignant pleural mesothelioma, and demonstrated that combination therapy of the chemotherapeutic agent pemetrexed with NZ-12 resulted in pronounced tumoricidal effects in xenograft mouse models of malignant pleural mesothelioma [18]. Based on these findings, these researchers proposed that the combination therapy pemetrexed with NZ-12 might offer therapeutic benefits for the treatment of individuals with malignant pleural mesothelioma [18]. All of these findings demonstrate how suitable a target antigen PDPN is and how it can be leveraged for therapeutic purposes. According to our findings, the conjugation of LpMab-2 to GrB is predicted to have no negative effects on the 3D structure of LpMab-2 or GrB, and the binding capacity and affinity of LpMab-2 to PDPN (despite lowering the solubility of LpMab-2 following its conjugation with GrB). In-depth analysis also indicated that both LpMab-2 and LpMab-2-(G_4S)3-GrB are projected to experience a slight loss of affinity to PDPN as the temperature increases from 25 to 37 ºC. This slight affinity decline might be important in the case of future applications since antibody conjugates are normally given to patients via systemic administration. However, future studies can focus on assessing the affinity of LpMab-2 to PDPN and LpMab-2-(G_4S)3-GrB to PDPN using precise techniques such as surface plasmon resonance. In-silico techniques employed in the current study could be used for the precise designing and development of antibody conjugates. Moreover, besides GrB, scFvs can also be easily engineered to be conjugated to various other cytotoxic agents such as toxins or chemical inhibitors. In a comparative view, scFvs are ~ 30 kDa while full-length mAbs are ~ 150 kDa; this renders scFv more capable of reaching tumor sites and reaching their target cells in comparison with full-length mAbs in the case of solid tumors.

5. Conclusion

Conjugation of mAbs and scFvs to cytotoxic agents could be explored for its therapeutic advantage. Herein, a PDPN-specific scFv conjugated to GrB, LpMab-2-(G_4S)3-GrB, was designed using precise *in-silico* techniques. *In vitro* experiments for the comparison of LpMab-2 with LpMab-2-(G_4S)3-GrB in terms of affinity, solubility, thermal stability, and other characteristics could shed more light on the applicability of LpMab-2-(G_4S)3-GrB. Moreover, assessing the antitumor efficacy of LpMab-2-(G_4S)3-GrB in preclinical xenograft mouse models of PDPN-expressing tumors could further validate the findings of this study.

Ethical Considerations

Compliance with ethical guidelines

There were no ethical considerations to be considered in this research

Funding

This research did not receive any grant from funding agencies in the public, commercial, or non-profit sectors.

Author's contributions

Conceptualization and Supervision, Methodology, Investigation, Writing – original draft, Writing – review & editing, Data collection, and Data analysis: Seyed Mohamad Javad Mirarefin.

Conflict of interest

The Authors declare that there is no conflict of interest.

Acknowledgments

We would like to extend our appreciation and thanks to all participants, staff, and managers who made this study possible.

References

[1] Sehn LH, Herrera AF, Flowers CR, Kamdar MK, McMillan A, Hertzberg M, et al. Polatuzumab Vedotin in Relapsed or Refractory Diffuse Large B-Cell Lymphoma. J Clin Oncol.2020;38(2):155-165. [DOI: 10.1200/JCO.19.00172] [PMID] [PMCID]

[2] Cortés J, Kim SB, Chung WP, Im SA, Park YH, Hegg R, et al. Trastuzumab Deruxtecan versus Trastuzumab Emtansine for Breast Cancer. N Engl J Med. 2022;386(12):1143-1154. [DOI: 10.1056/NEJMoa2115022] [PMID]

[3] Safarzadeh Kozani P, Safarzadeh Kozani P, Rahbarizadeh F. CAR T cells redirected against tumor-specific antigen glycoforms: can low-sugar antigens guarantee a sweet success? Front Med. 2022;16(3):322-338. [DOI: 10.1007/s11684-021-0901-2] [PMID]

[4] He Y, Schreiber K, Wolf SP, Wen F, Steentoft C, Zerweck J, Steiner M, Sharma P, Shepard HM, Posey A, June CH, Mandel U, Clausen H, Leisegang M, Meredith SC, Kranz DM, Schreiber H. Multiple cancer-specific antigens are targeted by a chimeric antigen receptor on a single cancer cell. JCI Insight. 2019;4(21):e130416. [DOI: 10.1172/jci.insight.130416] [PMID] [PMCID]

[5] Kato Y, Kaneko MK. A cancer-specific monoclonal antibody recognizes the aberrantly glycosylated podoplanin. Sci Rep. 2014;4:5924. [DOI: 10.1038/srep05924] [PMID] [PMCID]

[6] Rousalova I, Krepela E. Granzyme B-induced apoptosis in cancer cells and its regulation (review). Int J Oncol. 2010;37(6):1361-78. [DOI: 10.3892/ijo_00000788] [PMID]

[7] Ko J, Park H, Heo L, Seok C. GalaxyWEB server for protein structure prediction and refinement. Nucleic Acids Res. 2012 Jul;40(Web Server issue):W294-7. [DOI: 10.1093/nar/gks493] [PMID] [PMCID]

[8] Studer G, Rempfer C, Waterhouse AM, Gumienny R, Haas J, Schwede T. QMEANDisCo-distance constraints applied on model quality estimation. Bioinformatics. 2020;36(6):1765-1771. [DOI: 10.1093/bioinformatics/btz828] [PMID] [PMCID]

[9] Williams CJ, Headd JJ, Moriarty NW, Prisant MG, Videau LL, Deis LN, et al. MolProbity: More and better reference data for improved all-atom structure validation. Protein Sci. 2018;27(1):293-315. [DOI: 10.1002/pro.3330] [PMID] [PMCID]

[10] Bhattacharya D, Nowotny J, Cao R, Cheng J. 3Drefine: an interactive web server for efficient protein structure refinement. Nucleic Acids Res. 2016;44(W1):W406-9. [DOI: 10.1093/nar/gkw336] [PMID] [PMCID]

[11] Hebditch M, Carballo-Amador MA, Charonis S, Curtis R, Warwicker J. Protein-Sol: a web tool for predicting protein solubility from sequence. Bioinformatics. 2017;33(19):3098-3100. [DOI: 10.1093/bioinformatics/btx345] [PMID] [PMCID]

[12] Brenke R, Hall DR, Chuang GY, Comeau SR, Bohnuud T, Beglov D, Schueler-Furman O, Vajda S, Kozakov D. Application of asymmetric statistical potentials to antibody-protein docking. Bioinformatics. 2012;28(20):2608-14. [DOI: 10.1093/bioinformatics/bts493] [PMID] [PMCID]

[13] Kozakov D, Hall DR, Xia B, Porter KA, Padhorny D, Yueh C, Beglov D, Vajda S. The ClusPro web server for protein-protein docking. Nat Protoc. 2017;12(2):255-278. [DOI: 10.1038/nprot.2016.169] [PMID] [PMCID]

[14] Xue LC, Rodrigues JP, Kastritis PL, Bonvin AM, Vangone A. PRODIGY: a web server for predicting the binding affinity of protein-protein complexes. Bioinformatics. 2016;32(23):3676-3678. [DOI: 10.1093/bioinformatics/btw514] [PMID]

[15] Quintanilla M, Montero-Montero L, Renart J, Martín-Villar E. Podoplanin in Inflammation and Cancer. Int J Mol Sci. 2019;20(3):707. [DOI: 10.3390/ijms20030707] [PMID] [PMCID]

[16] Suzuki H, Kaneko MK, Kato Y. Roles of Podoplanin in Malignant Progression of Tumor. Cells. 2022;11(3):575. [DOI: 10.3390/cells11030575] [PMID] [PMCID]

[17] Shiina S, Ohno M, Ohka F, Kuramitsu S, Yamamichi A, Kato A, Motomura K, et al. CAR T Cells Targeting Podoplanin Reduce Orthotopic Glioblastomas in Mouse Brains. Cancer Immunol Res. 2016;4(3):259-68. [DOI: 10.1158/2326-6066.CIR-15-0060] [PMID]

[18] Abe S, Kaneko MK, Tsuchihashi Y, Izumi T, Ogasawara S, Okada N, et al. Antitumor effect of novel anti-podoplanin antibody NZ-12 against malignant pleural mesothelioma in an orthotopic xenograft model. Cancer Sci. 2016;107(9):1198-205. [DOI: 10.1111/cas.12985] [PMID] [PMCID]